The Journal of Experimental Biology 208, 929-938
Published by The Company of Biologists 2005
doi:10.1242/jeb.01433

Fast-start muscle dynamics in the rainbow trout *Oncorhynchus mykiss*: phase relationship of white muscle shortening and body curvature

Jeremy A. Goldbogen[1,*], Robert E. Shadwick[1], Douglas S. Fudge[2] and John M. Gosline[2]

[1]*Marine Biology Research Division, Scripps Institution of Oceanography, La Jolla, CA 92093-0204, USA* and [2]*Department of Zoology, University of British Columbia, 6270 University Boulevard, Vancouver, British Columbia V6T 1Z4, Canada*

*Author for correspondence (e-mail: jgoldbog@ucsd.edu)

Accepted 6 December 2004

Summary

Muscle length changes of the lateral myotomal fast fibers of rainbow trout (*Oncorhynchus mykiss*) were measured using sonomicrometry during induced fast-starts. Simultaneous high-speed videography allowed for the analysis of midline kinematics to estimate the degree of muscle strain that occurs during body deformation. Comparison of these data was used to examine the phase relationship between local muscle shortening and local body bending during unsteady, large amplitude maneuvers. Our analysis finds that muscle shortening is temporally decoupled from body bending, probably due to the influence of hydrodynamic forces. The phase shift was such that midline curvature lagged behind muscle shortening at both the anterior (0.4*L*, where *L* is fork length) and posterior (0.7*L*) axial positions. Stronger escape responses were correlated with high peak strains and rapid strain-wave velocities, but not faster curvature-wave velocities. Under these conditions of high strain, the phase shift at the posterior position is significantly increased, whereas the anterior position fails to be affected. Curvature lag was still observed at both axial locations under conditions of low strain, suggesting that hydrodynamic forces are still significant during weaker escape responses. These data support a previous model that suggests fast-start body bending is determined by the interaction between muscle torque and hydrodynamic resistance along the body.

Key words: trout, muscle strain, kinematics, *Oncorhynchus mykiss*, fast-start.

Introduction

Fast-starts are transient, high-acceleration maneuvers initiated at rest or imposed upon a period of steady swimming. This mode of locomotor behavior is critical for predatory avoidance or prey capture in a variety of fishes. The neurobiology, kinematics and muscle activity regarding fast-starts are relatively well understood (see Eaton et al., 1991; Jayne and Lauder, 1993; Domenici and Blake, 1997; Wakeling, 2001). Weihs (1973) categorized fast-starts into three kinematic stages: a preparatory bend to one side of the body (stage 1), a propulsive kick (stage 2) and a variable stage (stage 3). Subsequent researchers have refined the factors that define the transitions between stages according to EMG activity (Jayne and Lauder, 1993), onset of forward propulsion (Foreman and Eaton, 1993) and change in turning direction (Kasapi et al., 1993). Still, inherent variation of fast-start behavior both within and among individuals precludes the attempt to divide a continuous motion into distinct stages.

The Mauthner cells, a set of reticulospinal neurons that span the length of the spinal cord, typically mediate fast-starts (Eaton et al., 1991). Neural activation causes a nearly simultaneous impulse of muscle activity along the length of one side of the body (Jayne and Lauder, 1993; Wakeling and Johnston, 1999b; Ellerby and Altringham, 2001; Tytell and Lauder, 2002) that results in a concomitant onset of muscle strain at all axial locations (Ellerby and Altringham, 2001). However, some basal actinopterygians exhibit strong muscle activation on both sides of the body (Westneat et al., 1998; Tytell and Lauder, 2002). Despite the simultaneous onset of muscle activity and muscle strain, actual body bending occurs as a posteriorly traveling wave because of the morphologically derived axial variation in muscle torque and hydrodynamic resistance (Wakeling and Johnston, 1999b). In addition, the faster shortening velocities of the rostral myotomes function to generate stress more rapidly than at more posterior locations (James et al., 1998; Johnston et al., 1993, 1995; Wardle et al., 1989; Altringham et al., 1993; Davies et al., 1995; Wardle, 1985). Consequently, the fast myotomal muscle produces a net bending moment on the spine, curving the body to the ipsilateral (concave) side of the body that signifies the completion of stage 1 in most fast-starts. Stage 2 is associated with a wave of muscle activity generated on the contralateral (convex) side of the body (Jayne and Lauder, 1993; Wakeling and Johnston, 1999b; Hale et al., 2002), producing a propulsive flexion and a rapid acceleration away from the stimulus.

Although the muscle activity during fast-starts is relatively well understood, there are few detailed studies that focus on the changes in muscle length that produce these rapid bending and propulsive moments. Recent investigations regarding the muscle dynamics of steady swimming have provided evidence that the wave of muscle shortening traveling along the body is in phase with changes in local midline curvature, as in a homogeneous bending beam (Coughlin et al., 1996; Shadwick et al., 1998; Katz et al., 1999; Donley and Shadwick, 2003). These results were qualitatively consistent, at an unspecified axial location, in common carp fast-starts (Wakeling and Johnston, 1999a). However, studies involving the deep red muscle of steady swimming in the shortfin mako shark (Donley et al., 2004) and tunas (Shadwick et al., 1999; Katz et al., 2001) have shown a temporal decoupling of muscle length and backbone kinematics, such that muscle shortening in the mid-body region is in phase with curvature at more posterior locations. The first measurement of muscle length changes during fish fast-starts (Covell et al., 1991) led to a similar conclusion, but the analysis highlighted muscle dynamics only in relation to total body curvature. Thus, it is not clear how white muscle shortens to create body bending during maximal performance.

Since the pioneering study by Covell et al. (1991), substantial advances have been made regarding the kinematic analysis of fish locomotion, particularly aided by digital techniques (Jayne and Lauder, 1995; Katz and Shadwick, 1998; Walker, 1998). In the present study, we revisit the phase relationship between muscle strain and midline curvature in the fast-start behavior of *Oncorhynchus mykiss* to address the incongruence in our understanding of fish swimming mechanics. We used sonomicrometry to measure shortening in the lateral myotomal fast fibers during induced escape responses. Simultaneous high-speed video analysis was used to calculate local midline curvature and estimate the strain experienced during the observed body deformation. We compare these data to examine the phase relationship between local muscle shortening and midline curvature.

Materials and methods

Experimental protocol and animals

Six rainbow trout *Oncorhynchus mykiss* (Walbaum), ranging in size from 31 to 34 cm fork length (*L*), were obtained from a hatchery and housed in a circular 1,000 l aquarium at 15–20°C. Experiments on these individuals were performed in a rectangular, plexiglass tank (2.45 m × 1.22 m × 0.47 m) that contained a 10 cm grid to facilitate the calibration of captured film images.

The experimental tank was filled to a depth of 30 cm such that the maneuver was largely within the horizontal plane. Fast-starts were induced from rest by jabbing a meter stick vertically into the experimental tank towards the fish. Over the course of the study, several escape responses were recorded for each individual, which ranged from very strong responses where the head often touched the tail to very weak responses.

Implantation of piezoelectric crystals for *in vivo* measurement of white muscle strain required that the individual be anesthetized. In preparation for surgery, each fish was exposed to tricane methanesulfonate (MS222; Sigma Chemical Co., St Louis, MO, USA) (0.0001 kg l^{-1} buffered with Tris HCl) to induce a short period of anesthesia (<30 min). The gills were continuously perfused with anesthetic during surgery and subsequently flushed with fresh water to facilitate recovery. Fish were allowed to recover in isolation chambers for at least 24 h before the experiment was performed.

Sonomicrometry and muscle strain

Two pairs of 1.0 mm diameter piezoelectric crystals were inserted into the deep, interior white (epaxial lateral) muscle at two axial locations (0.4*L* and 0.7*L*) along one side of each fish. Each pair of crystals (1 cm apart and parallel to the longitudinal axis of the animal) was oriented approximately 10–20 mm dorsal of the horizontal septum and 4–9 mm lateral of the spine (approximately centered in the middle of epaxial cones). Wires leading to the crystals were bundled and sutured to the skin. Axial locations were highlighted by reflective markers that were glued to the dorsal surface of the fish (see Fig. 1). Sonometric data were obtained with a digital sonomicrometer at 250 Hz during induced fast-start maneuvers. Muscle length traces allowed for the calculation of muscle strain (ε_S):

$$\varepsilon_S = \Delta l / l_0 ,$$

where Δl is the change in length and l_0 is the resting muscle length. Following the experiment, the exact location of the piezoelectric crystals was revealed by postmortem dissection. The sonometric data were not filtered or smoothed for analysis.

Kinematic analysis, curvature and predicted strain

Dorsal views of elicited escape responses were captured with a high-speed video camera (Redlake; San Diego, Ca, USA) at a filming frequency of 250 Hz. The dorsal–ventral projected outline of the fish was digitized on each frame using NIH Image (National Institutes of Health, http://rsb.info.nih.gov/nih-image). These outlines were used to calculate a dorsal midline consisting of 51 equidistant coordinates that characterize 50 equally spaced segments (see Jayne and Lauder, 1995). Midline coordinates allowed for local curvature (*K*), the inverse of the radius of curvature, to be estimated at axial positions corresponding to each crystal position with QuicKurve (Walker, 1998), using a quintic spline function (M=3) and a smoothing parameter of 25 (*MD*=1). Maximum curvature was selected as the maximum curvature experienced at a particular location along the body over the course of the fast-start maneuver. Predicted strain, or estimated strain (ε_K), was calculated as the product of local curvature (*K*) and the lateral distance from the backbone to the piezoelectric crystals (*h*), just as in a simple beam (see Rome et al., 1988; Van Leeuwen et al., 1990):

$$\varepsilon_K = Kh .$$

Phase shift

The sonometric and video data were synchronized by a trigger that produced a voltage spike on a separate data channel and simultaneously stopped recording video frames. The temporal relationship between measured strain and midline curvature (i.e. estimated strain) was quantified using a cross-correlation analysis. This method involves the calculation of the coefficient of determination, which describes how closely the measured values correspond to the estimated values. Profiles were then shifted with respect to one another to find the time change required to maximize the coefficient of determination.

Wave velocity

The velocities at which strain and curvature waves propagated along the body were calculated by dividing the distance between the posterior and anterior sample sites by the travel time of the corresponding wave minima (muscle shortening and concave curvature) or maxima (muscle lengthening and convex curvature).

Turning rate

Turning rate of the head during fast-starts were calculated following the methods of Domenici et al. (2004). An angle was formed between the head, a point on the midline at 0.33*L* and

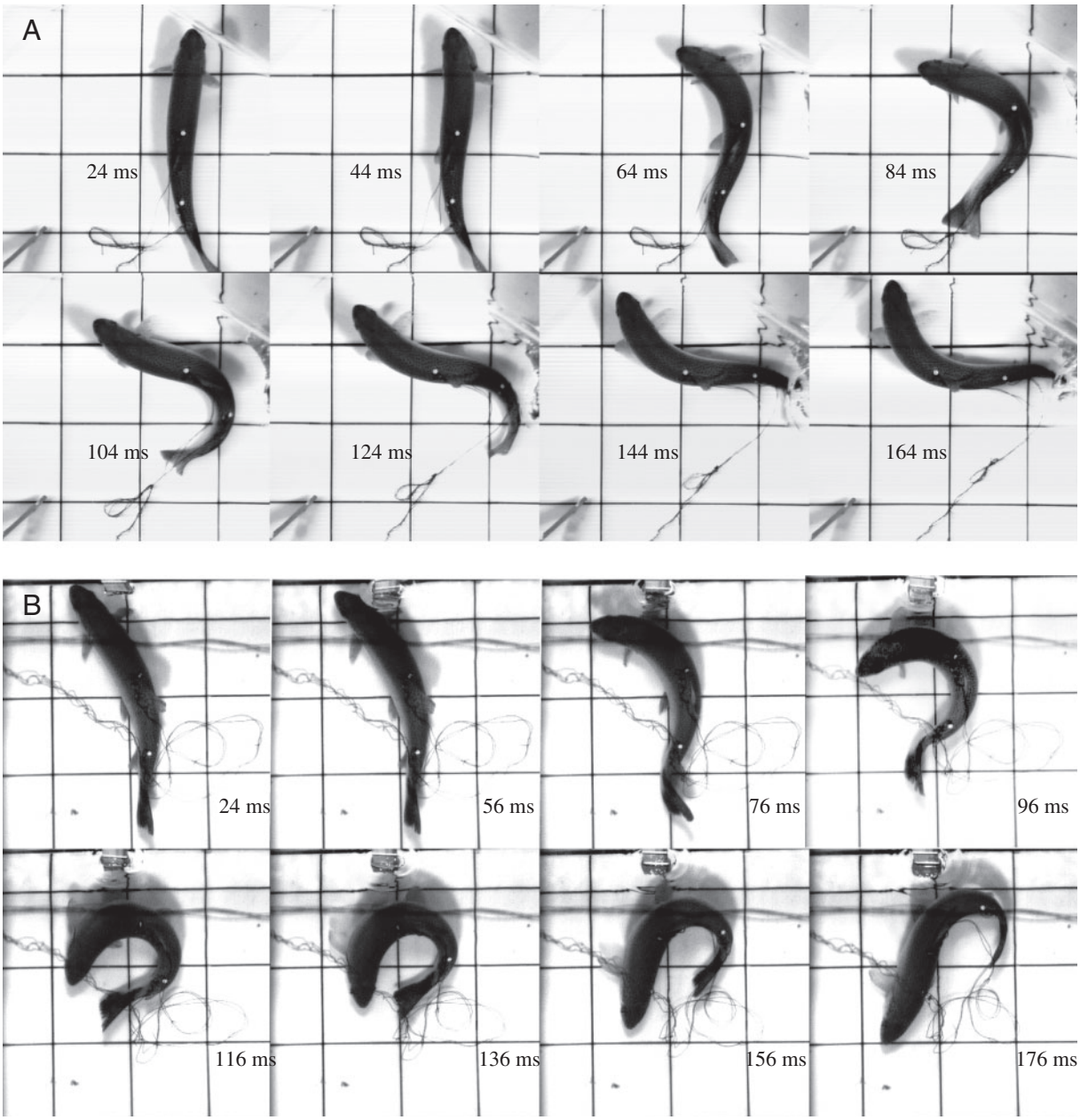

Fig. 1. Sequential frames from high-speed videography (250 Hz) during induced fast-starts. A representative example of a response under low strain (A) and a response under high strain (B). Markers are visible on the back of the fish at 0.4*L* and 0.7*L*.

a reference axis. Turning rates were calculated by how this angle changed over time.

Total body curvature in relation to strain

For the purposes of analyzing the phase relationship between midline curvature and muscle shortening under different degrees of strain, the average strain between the anterior and posterior position was calculated for each response. The average of this value for all individuals and trials, 12.3%, was set as the arbitrary boundary between low strain (<12.3%) and high strain (>12.3%) events. We emphasize that this categorization does not suggest that *O. mykiss* exhibits two distinct behavioral response types. Rainbow trout probably exhibit a continuum of escape responses from weak to strong, but quantification of this would require a comprehensive behavioral study. The division used in this study allows us to investigate white muscle dynamics under different mechanical conditions.

To estimate total body curvature, the minimal distance between the head and caudal peduncle was recorded over the course of the maneuver (see Brainerd and Patek, 1998). Therefore, smaller distances reflected larger total body curvatures. This parameter is meant to be an index of total body curvature not an absolute quantity.

Statistics

All statistical analyses were performed using Minitab (version 13; Minitab Inc., State College, PA, USA) with a significance level of P=0.05. All parameters failed the Anderson-Darling test for normality ($P<\alpha$). Thus, the following non-parametric statistical analyses were warranted.

A Wilcoxon signed rank test was performed to determine if the phase shift between measured strain and estimated strain was different than zero. A P-value <0.05 accepts the hypothesis that the compared values are significantly different than zero. To account for a combined error of one frame for the sonometric and kinematic data, the Wilcoxon point estimate was adjusted to 0.004 s.

A Mann-Whitney U-test was used to test whether the kinematic parameters between high and low strain events were significantly different. A P-value <0.05 accepts the hypothesis that the two parameters are significantly different.

Results

Midline kinematics

All observations on the muscle dynamics in this study involved the deep, interior white muscle during induced escape responses (six individuals, 20 trials). Of these six individuals, two individuals exhibited responses under both high and low strain conditions, two individuals exhibited responses under only low strain conditions, and two individuals exhibited responses under only high strain conditions. Sample sizes did not permit a test for an effect on individuals.

A representative example of an escape response under high and low strain conditions is shown in Fig. 1. The midline kinematics over the course of each response type is shown in Fig. 2. Qualitatively, the weaker response is similar to the '*L*-start without a turn' pattern and the stronger response type is similar to the '*L*-start acceleration turn' pattern described previously for the rainbow trout, *Salmo gairdneri* (Webb, 1976). For lack of muscle activation data during these fast-starts, we defined kinematic stages of fast-starts by a change in turning direction (see Kasapi et al., 1993). Low strain responses exhibited a much smaller ipsilateral bend during stage 1, whereas high strain responses usually involved much tighter c-shape profiles at the end of stage 1 (Figs 1–3).

The calculation of curvature along the backbone revealed a profile that describes the maximum curvature experienced over

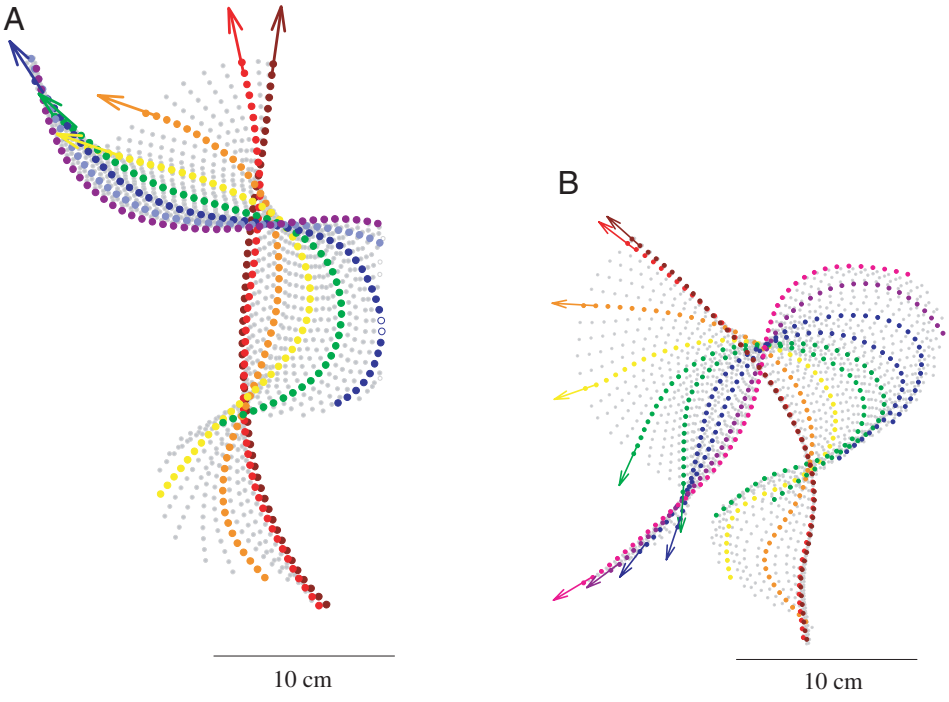

Fig. 2. Midline kinematics in x–y coordinate space derived from the digitized outlines of each video frame (250 Hz). Colored circles correspond to each video frame shown in Fig. 1 for a response under low strain (A) and a response under high strain (B), starting with dark red colors and progressing through the colors of the rainbow to violet. Arrows denote orientation of the head as an extension of the first two digitized segments.

the course of the maneuver (Fig. 4). Maximum curvature increases sharply between approximately 0.1*L* and 0.3*L* and decreases between 0.9*L* and 1.0*L*, both of which are a consequence of an anatomical limitation to bending at the extreme ends of the fish. For example, the head lacks vertebrae and the extreme end of the tail is completely devoid of muscle. In the central region of the body (0.3*L* to 0.9*L*) maximum curvature generally increases, but includes local minima. It should be noted that calculations of curvature assumed that the long axis of all cross sections of the fish remained vertically orientated. Thus, escape responses may have involved roll moments (see Fig. 1B), which may cause curvature to be slightly under- or over-estimated depending on the direction of rotation.

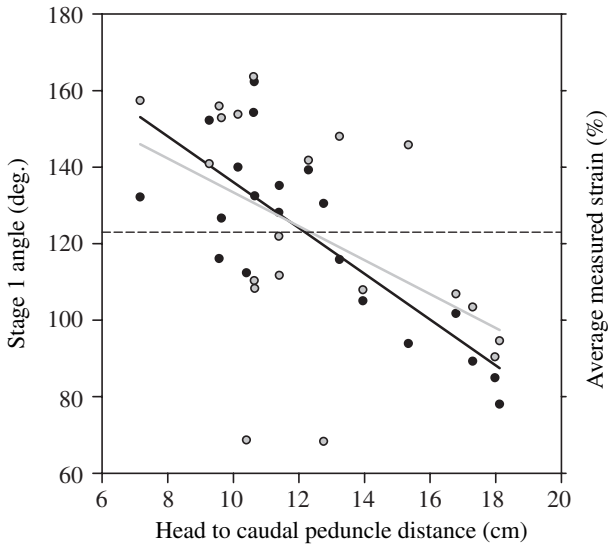

Fig. 3. Stage 1 angle (dark circles) and the average measured peak strain between the anterior and posterior axial positions (gray circles) expressed as a function of the minimum distance measured between the head and caudal peduncle (an index of total body curvature, where smaller distances are interpreted as greater overall curvatures) over the course of the escape response. The dashed line (12.3% average strain) corresponds to the arbitrary division used to separate high strain and low strain events.

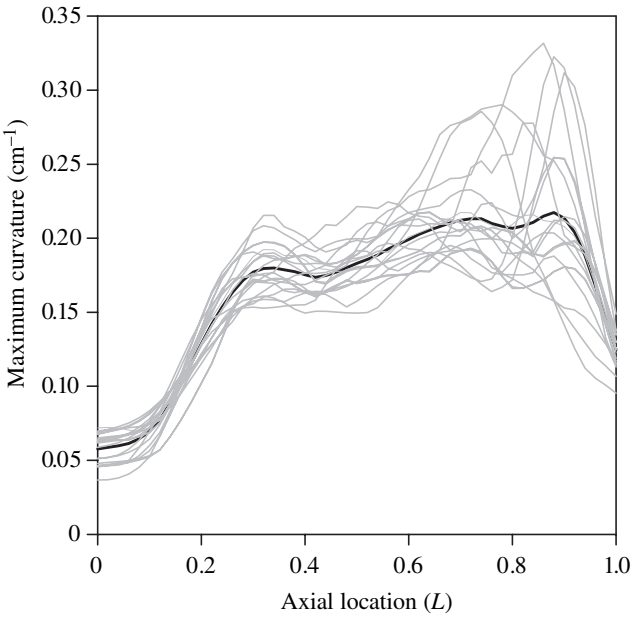

Fig. 4. Maximum curvature experienced along the length of the body during 20 fast-starts of six fish. Axial location runs from the tip of the head (0.0*L*) to the tail (1.0*L*). Gray profiles denote individual trials and the black profile shows the mean curvature. Note the local minimum at approximately 0.4*L*.

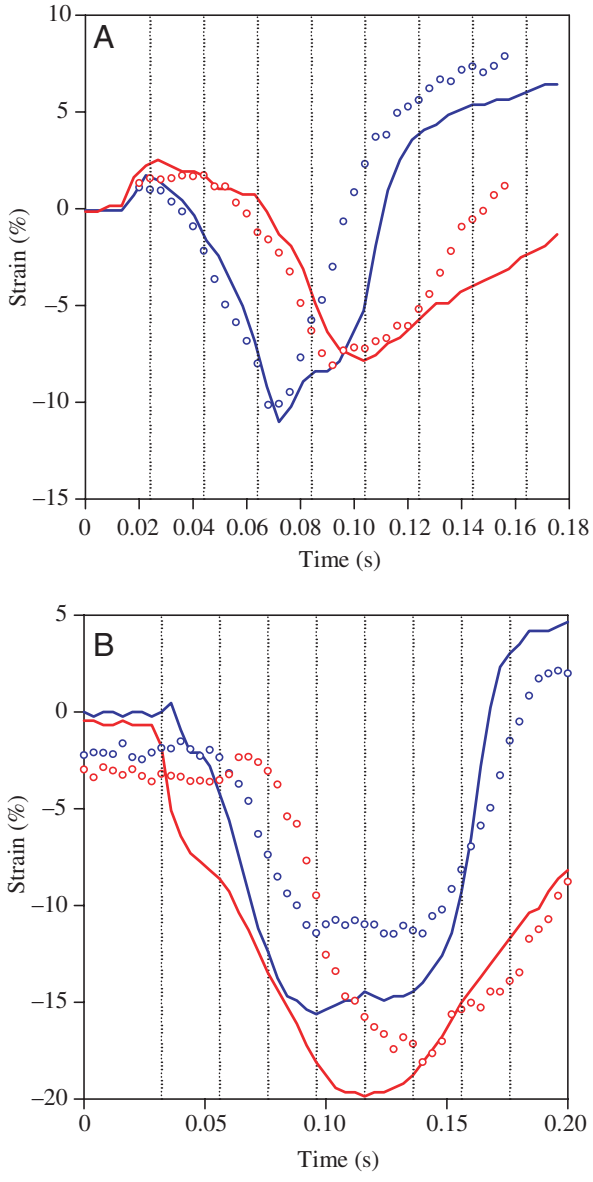

Fig. 5. Time series of measured strain (solid lines) from sonomicrometry and predicted strain (open circles) from midline curvature for the anterior (blue) and posterior (red) positions. Vertical dashed lines represent sequential video frames shown in Fig. 1 for a weaker response (A) and a stronger response (B). Sonometric crystals are located on the concave side of the bend for each response and, thus, show muscle shortening.

Table 1. *Kinematic parameters calculated for trout fast-starts*

Variable	Low strain	High strain	Test
Anterior strain measured from sonomicrometry (%)	10.3±3.4 (4.6–13.4)	15.1±4.8 (6.7–20.6)	$P<0.05$
Posterior strain measured from sonomicrometry (%)	8.8±3.0 (5.3–15.7)	19.0±6.0 (13.4–31.1)	$P<0.005$
Anterior strain predicted from beam theory (%)	10.8±1.0 (9.7–12.8)	11.2±1.1 (10.1–13.1)	$P=0.287$
Posterior strain predicted from beam theory (%)	10.2±2.5 (5.3–15.7)	12.4±2.7 (13.4–31.1)	$P=0.149$
Anterior measured strain – anterior predicted strain (%)	–0.5±3.1 (–6.1–2.8)	3.9±5.0 (–4.6–9.4)	$P=0.575$
Posterior measured strain – posterior predicted strain (%)	–1.5±3.9 (–8.5–5.6)	6.6±6.6 (1.2–20.0)	$P<0.005$
Anterior phase shift (s)	0.007±0.006 (0–0.016)	0.006±0.005 (0–0.012)	$P=0.784$
Posterior phase shift (s)	0.005±0.005 (0–0.012)	0.021±0.009 (0.008–0.040)	$P<0.005$
Strain wave velocity (L s^{-1})	11.2±1.6 (9.4–15.0)	30.9±25.61 (10.7–75.0)	$P<0.005$
Curvature wave velocity (L s^{-1})	11.7±4.3 (6.3–18.8)	15.9±8.4 (4.7–25.0)	$P=0.358$

Kinematic parameters calculated during induced fast-starts (20 trials, six individuals). Escape responses are categorized into high strain (>12.3%; nine trials, four individuals) and low strain (<12.3%; 11 trials, four individuals) events. Strain values correspond to peak strains experienced during the maneuver. Phase shift describes the time change that maximizes synchrony between measured and predicted strain profiles. Strain wave and curvature wave velocities were calculated by dividing the distance between the two sample sites by the time between the associated wave maxima/minima.

Values are means ±S.D. and ranges are included in parentheses. All statistical tests were Mann-Whitney U-tests to determine whether each parameter was not equal between high strain and low strain events.

Measured and predicted strain

Measured strain from sonomicrometry and predicted strain from midline curvature recorded for a high and low strain event are shown in Fig. 5. Escape responses occurred with piezoelectric crystals implanted either on the ipsilateral or contralateral side of the escape response. Thus, our analysis involved either muscle lengthening (one of nine strong responses, four of 11 weak responses) or muscle shortening. Since the crystals were too often (eight of nine responses) on the convex side of the body during strong responses, passive muscle lengthening in relation to midline curvature could not be analyzed under high strain.

Several kinematic parameters for high and low strain events are listed in Table 1. For all escape responses, peak muscle strains measured by sonomicrometry ranged from 4.6–20.6% at 0.4L and 5.3–31.1% at 0.7L, while strain calculated from curvature and chordwise crystal position ranged from 9.7–13.1% at 0.4L and 7.3–18.1% at 0.7L (see Table 1 for means and standard deviations). Measured strain was significantly higher for strong responses at both axial positions, whereas predicted strain was not significantly different between responses for either position. The difference between measured and predicted strain was only significantly higher for high strain events at the posterior position. The comparison between measured and estimated strain (including peak, initial and final strain) for both axial positions is shown in Fig. 6. The slope of the regression line through the data is similar to unity, which suggests *O. mykiss* fast-starts can be generally described as a simple bending beam.

The onset of muscle length change at both the anterior and posterior locations occurred simultaneously (Fig. 5), but there was a time delay to reach minimum or maximum length yielding an average strain wave speed of 20.6±19.8 L s^{-1} for all trials. Strain wave velocities were significantly higher for high strain events while curvature wave velocities remained constant (Table 1). Accordingly, changes in midline curvature often lagged behind the onset of muscle shortening (Fig. 5B).

Phase shift

Comparison of measured and predicted strain profiles shows a clear temporal relationship (Fig. 5), but this association was not always perfectly in phase. In cases where this phase shift was not zero, measured strain always preceded curvature. The

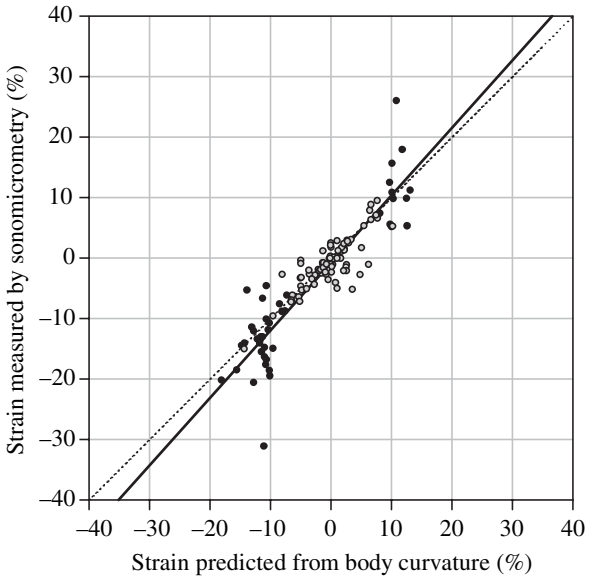

Fig. 6. White muscle strains measured by sonomicrometry at both axial locations (0.4L and 0.7L) closely match strains estimated from body curvature, but this trend deviates at higher strains. Peak (black circles), initial and final (gray circles) strains were measured during induced fast-starts. The solid line represents the linear regression through initial, peak and final strains (r^2=0.82, $P<0.05$). The strain relationship of a homogeneous bending beam is expressed by the dashed line.

average phase shift for the anterior position was 0.006±0.005 s and was significantly different from zero (Wilcoxon Signed Rank Test, P=0.033). The average phase shift for the posterior position was 0.012±0.011 s and was significantly different from zero (Wilcoxon Signed Rank Test, P=0.002).

The escape response under high strain in Fig. 5B shows a large temporal decoupling between measured and predicted strain at the posterior location. The effect of high strain on phase shift is shown in Fig. 7. High strain significantly increases the phase shift at the posterior location to an average of 0.021±0.009 s (Mann-Whitney U-Test, P<0.005). High strain also affects the magnitude of the measured strain experienced between the anterior and posterior positions such that they are negatively correlated (Fig. 8). In contrast, conditions of high strain fail to affect the anterior phase shift (Mann-Whitney U-Test, P=0.784, Fig. 7). Stronger escape responses appear to be a consequence of rapid strain wave velocities (Table 1), which in effect cause muscle length minima at the anterior and posterior locations to occur closer in time while hydrodynamic resistance causes curvature to lag.

Discussion

In a previous study involving trout fast-starts, Covell et al. (1991) described a temporal decoupling between the onset of muscle shortening and total body curvature, such that curvature preceded muscle shortening at several sites along the body.

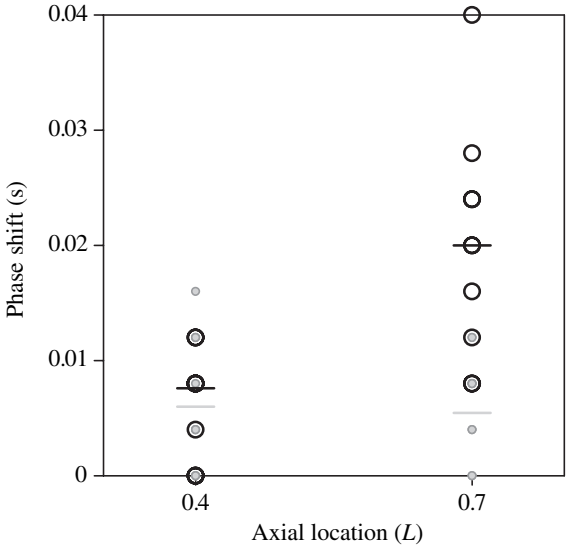

Fig. 7. The effect of high strain on the phase shifts between measured and estimated strain during induced fast-starts for the anterior (0.4*FL*) and posterior (0.7*FL*) locations. Stronger escapes (11 trials, four individuals), which experience an average strain between the anterior and posterior position greater than 12.3%, are represented by black open circles and average phase shifts are represented by horizontal black bars. Weaker escapes (nine trials, four individuals), less than 12.3% average strain, are shown by gray-filled circles and average phase shifts are represented by horizontal gray bars. High strain significantly increases the average phase shift from 0.005±0.005 s to 0.021±0.009 s at 0.7L (Mann-Whitney U-test, P<0.005).

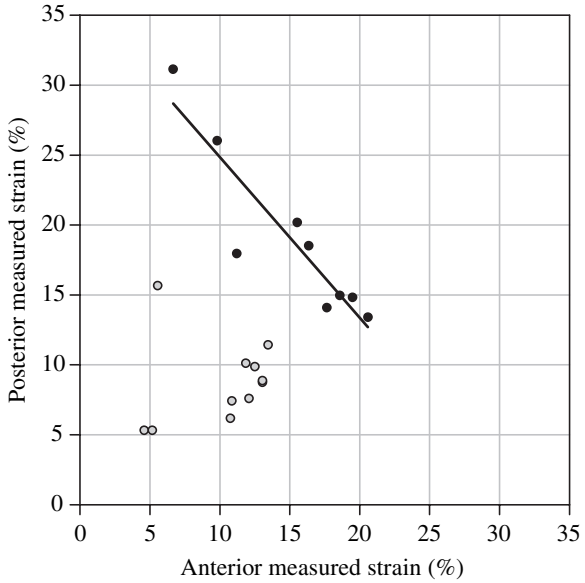

Fig. 8. Comparison between measured peak strain at the anterior (0.4*FL*) and posterior (0.7*FL*) positions for each response. High strain events (>12.3%) are shown by black circles, whereas low strain events (<12.3%) are shown by gray circles. A linear regression of the data is shown for high strain events (P<001, r^2=0.84, N=9).

Our analysis modifies these conclusions by demonstrating a simultaneous onset of muscle shortening, as was found in *O. mykiss* fast-starts (Ellerby and Altringham, 2001) and changes in local body curvature. Our results also show a temporal decoupling of minimum muscle length at different sites along the body, agreeing with Ellerby and Altringham (2001), but disagreeing with Covell et al. (1991) who found no time delay in minimum muscle length across a smaller axial distance of 0.19L. Indeed, comparing muscle length changes between two relatively close sites will make a rapidly traveling strain wave difficult to detect (Ellerby and Altringham, 2001).

Our analysis of fast-start muscle dynamics in *O. mykiss* fast-starts shows a temporal decoupling between contractions of white muscle fibers and changes of local midline curvature. This phase shift was observed to significantly increase under conditions that yielded high strain at the posterior axial location (0.7L). The phase shift observed at the anterior region (0.4L) was not affected by high strain, but a significant curvature lag was still observed. This dichotomy suggests that differential hydrodynamic resistance is the primary mechanism underlying this phase shift. This hypothesis is consistent with the fact that body bending is increasingly resisted by hydrodynamic resistance along the body in the posterior direction (Wakeling and Johnston, 1999b), and that hydrodynamic thrust is imparted to the water primarily through the caudal region (Weihs, 1973; Webb, 1977; Frith and Blake, 1991).

Regardless of response strength, the tendency of muscle shortening to precede local midline curvature highlights the significance of external resistance during fast-starts. For steady

swimming, similar effects may not be significant considering that relatively high strains are rarely observed during this swimming mode. Katz et al. (1999) described one instance during burst swimming in milkfish where curvature lagged behind red anterior (0.53*L*) muscle shortening by 16.7 ms under relatively high strain (approximately 13%). However, red muscle in the same trial at the posterior location (0.71*L*) also reached strains of about 13%, but resulted in muscle shortening lagging behind curvature. All other studies that have compared local body bending with local muscle length changes have involved relatively low strain regimes (Coughlin et al., 1996; Shadwick et al., 1999; Donley and Shadwick, 2003; Donley et al., 2004).

For steady swimming and fast-starts in most fish, axial strain magnitude from simple beam theory appears to be an accurate predictor of strain measured by sonomicrometry (Coughlin et al., 1996; Katz et al., 1999; Wakeling and Johnston, 1999a; Long et al., 2002). Beam theory is time independent (steady state) and involves homogeneous, linearly elastic material (Stevens, 1987). Therefore, this beam-like behavior in swimming fish muscle is unexpected given that the myotendinous machinery of fishes is incredibly complex (Gemballa and Vogel, 2002). In addition, undulatory swimming relies on reactive forces generated from lateral accelerations of a given body segment (Daniel, 1984). Peak measured and predicted strains from this study are compared with data from several species performing various swimming behaviors (Fig. 9). This comparison shows that only the posterior position under high strain departs from beam theory predictions. The deviation is similar to that observed in tunas where strain from sonomicrometry is greater than strain estimated from beam theory. Interestingly, this position and condition (posterior, high strain) also exhibits the highest phase shift (Fig. 7). In this way, beam theory can be used to estimate hydrodynamic forces along the body by demonstrating incongruence between measured and predicted strain.

The nature of the phase shift in this study is unlike that found in tunas and the shortfin mako shark where muscle shortening at a given location was found to be in phase with curvature at a much more posterior location (Shadwick et al., 1999; Donley et al., 2004). These phase shifts are a mechanical consequence of the highly specialized myotendinous architecture in these fishes whereas the curvature lag in fast-starts is probably a result of hydrodynamic forces. Thus, white muscle in fast-starts of *O. mykiss* acts locally to generate a posteriorly directed wave of body bending, but during maximal performance a hydrodynamic limit to large and rapid lateral deflection is imposed. The mechanism by which muscle shortens in advance of local bending, as we present here, likely involves muscle or connective tissue deformation at another location. In some video sequences the length of the entire body was observed to shorten just prior to the escape maneuver (Fig. 1B), most notably in the head region; however, the resolution of our analysis was not sufficient to quantify this change.

Furthermore, localized contraction without body bending could cause shearing (Alexander, 1969), which would potentially depress the development of local curvature (see Fig. 4). Local minima can also be observed in maximum curvature profiles for several other species performing fast-starts (Wakeling and Johnston, 1998; Fernandez et al., 2002). When a beam is flexed, the concave side develops compressive stress while the convex side experiences tensile stress. The application of these antagonistic forces on each segment of the beam can cause either rotation or shear (Vogel, 2003). The angular acceleration of spine bending was shown to sharply decrease from approximately 0.2*FL* to 0.4*FL* in common carp escape responses (Wakeling and Johnston, 1999b). Given this circumstance the body segment must shear. The proportion of shear to rotation that occurs is likely to be a function of vertebral length, where few long vertebrae enhance shear and many small vertebrae are more likely to rotate (J. M. Wakeling, personal communication). These speculations warrant the investigation of three-dimensional muscle deformation during fish locomotion.

Our results support Wakeling and Johnston's (1999b) model that explains fast-start body bending in terms of muscle torque

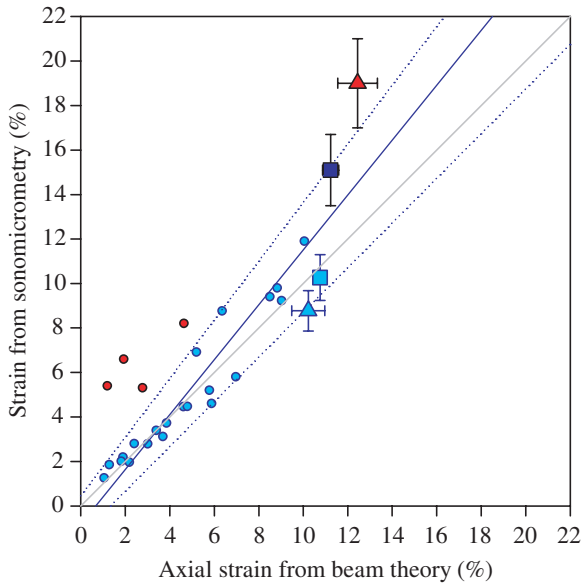

Fig. 9. Strain magnitude calculated from simple bending beam theory accurately predicts axial strain measured by sonomicrometry (blue line; P=0.0001; r^2=0.9163; N=22). Blue circles represent observations from steady swimming, fast-starts, and sprinting in several species of fish (Coughlin et al., 1996; Katz et al., 1999; Wakeling and Johnston, 1999; Ellerby and Altringham, 2001). Tuna steady swimming, represented by red circles, are excluded from the regression because of their specialized myotendinous architecture (Shadwick et al., 1999; Katz et al., 2001). Fast-start data from this study are superimposed onto this figure: strains calculated at the anterior position (squares) and the posterior position (triangles) are shown for weaker responses (light blue) and stronger responses (dark blue and red). Note that only the posterior location under high strain lies outside the 95% confidence interval that contains the one-to-one predictor (gray line). Standard errors of the mean are only shown for the present study for brevity. Figure adapted from Long et al. (2002).

and hydrodynamic resistance. The large muscle mass in the anterior region provides high power (Wakeling and Johnston, 1999b) and high stiffness (Blight, 1977; Wainright et al., 1978; Westneat et al., 1998), while the reduction of muscle mass in the posterior region contributes low power and low stiffness (Blight, 1977). Strong bilateral muscle activity may also serve to increase body stiffness in a time dependent manner (Westneat et al., 1998), but this neuromuscular pattern is not observed in *O. mykiss* (Hale et al., 2002). However, stage 1 body bending is sufficiently explained by muscle torque alone, even with internal stiffness making no contribution (Wakeling and Johnston, 1999b). Additionally, curvature wave velocities along the body were found to be independent of stage 1 bilateral muscle activity in the bichir *P. senegalus* (Tytell and Lauder, 2002). Therefore, a more appropriate hybrid oscillator model for a bending fish would describe the anterior region as torque dominated rather than stiffness dominated. This hypothesis is reinforced by the observation in this study that muscle segment shortening rate and head turning rate maxima at 0.4*L* are closely associated (Fig. 10). This suggests that head turning is a consequence of bending moments driven by torques generated in the anterior region. It appears as though a stiffer anterior region is better equipped to turn and cut through the medium. Conversely, a more flexible posterior region seems aptly designed to impart momentum to the water by maximizing reactive forces, particularly by effecting the shape dependence of the acceleration reaction.

As torque decreases along the body (Wakeling and Johnston, 1999b), hydrodynamic resistance to lateral deflection increases largely due to the presence of a caudal fin, which adds substantial added mass and increases external resistance to lateral acceleration (Weihs, 1973). A robotic simulation by Ahlborn et al. (1997) showed that increasing the delay between initial and return strokes generates maximal thrust. The propulsive forces associated with the change in rotational momentum (Albhorn et al., 1991) may be enhanced by a resistance dominated posterior region. This mechanical property could passively act as an excellent transmitter of posteriorly directed forces, especially considering the longitudinal orientation of posterior muscle fibers and tendinous structures (Gemballa and Vogel, 2002). As force is projected caudally, a sufficient time period is provided for vorticity to develop around the caudal fin. Clearly, more empirical hydrodynamic analyses (e.g. Wolfgang et al., 1999) of wake structure during fast-starts of real fish are needed before any firm conclusions can be made.

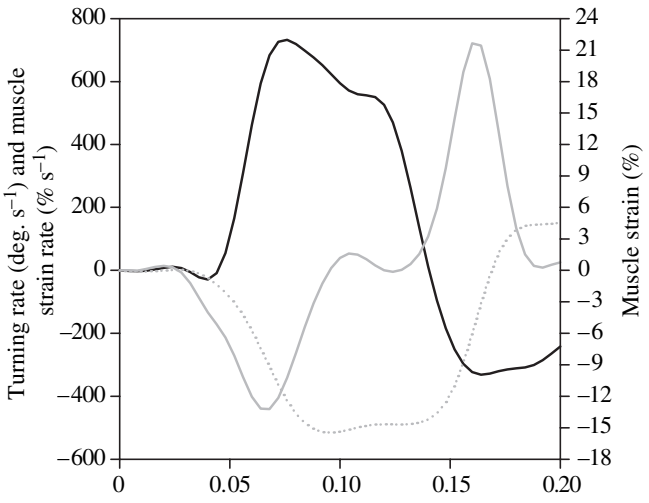

Fig. 10. Muscle strain rate (gray line) minimum at 0.4*L* is coincident with the rapid increase in head turning rate (black line). Muscle strain rate was derived from the muscle strain profile shown by the dotted gray line.

We thank John Long for permission to use a previously published figure as a template for Fig. 10 in this manuscript. We thank Robert Blake for providing lab facilities for the study. We thank George Lauder and Jeffrey Walker for providing computer software that aided in the kinematic analysis of video data. One anonymous reviewer provided helpful comments on beam theory. Brendan Borrell, Jeanine Donley, Torre Knower, Megan McKenna, Jessica Meir, and James Wakeling provided useful comments on the manuscript. This project was supported by funding from the National Science Foundation IBN-0091987.

References

Ahlborn, B., Harper, D. G., Blake, R. W., Ahlborn, D. and Cam, M. (1991). Fish without footprints. *J. Theor. Biol.* **148**, 521-534.

Ahlborn, B., Chapman, S., Stafford, R. and Harper, R. (1997). Experimental simulation of the thrust phases of fast-start swimming of fish. *J. Exp. Biol.* **200**, 2301-2312.

Alexander, R. M. (1969). The orientation of muscle fibers in the myomeres of fishes. *J. Mar. Biol.* **49**, 263-290.

Altringham, J. D., Wardle, C. S. and Smith, C. I. (1993). Myotomal muscle function at different locations in the body of a swimming fish. *J. Exp. Biol.* **182**, 191-206.

Blight, A. R. (1977). The muscular control of vertebrate swimming movements. *Biol. Rev.* **52**, 181-218.

Brainerd, E. L. and Patek, S. N. (1998). Vertebral column morphology, c-start curvature, and the evolution of mechanical defenses in tetraodontiform fishes. *Copeia*. **4**, 971-984.

Coughlin, D. J., Valdes, L. and Rome, L. C. (1996). Muscle length changes during swimming in scup: sonomicrometry verifies the anatomical high-speed cine technique. *J. Exp. Biol.* **199**, 459-463.

Covell, J. W., Smith, M., Harper, D. G. and Blake, R. W. (1991). Skeletal muscle deformation in the lateral muscle of the intact rainbow trout *Oncorhynchus mykiss* during fast start maneuvers *J. Exp. Biol.* **156**, 453-466

Daniel, T. L. (1984). Unsteady aspects of aquatic locomotion. *Am. Zool.* **24**, 121-134.

Davies, M. L. F., Johnston, I. A. and van de Wal, J. (1995). Muscle fibers in rostral and caudal myotomes of the Atlantic cod (*Gadus morhua* L.) have different mechanical properties. *Physiol. Zool.* **68**, 673-697.

Domenici, P. and Blake, R. W. (1997). The kinematics and performance of fish fast-start swimming. *J. Exp. Biol.* **200**, 1165-1178.

Domenici, P., Standen, E. M. and Levine, R. P. (2004). Escape manoeuvers in the spiny dogfish (*Squalus acanthias*). *J. Exp. Biol.* **207**, 2339-2349.

Donley, J. M. and Shadwick, R. E. (2003). Steady swimming muscle dynamics in the leopard shark *Triakis semifasciata. J. Exp. Biol.* **206**, 1117-1126.

Donley, J. M., Sepulveda, C. A., Konstantinidis, P., Gemballa, S. and Shadwick, R. E. (2004). Convergent evolution in mechanical design of lamnid sharks and tunas. *Nature* **429**, 61-65.

Eaton, R. C., DiDomenico, R. and Nissanov, J. (1991). Role of the mauthner cell in sensorimotor integration by the brain stem escape response. *Brain Behav. Evol.* **37**, 272-285.

Ellerby, D. J. and Altringham, J. D. (2001). Spatial variation in fast muscle function of the rainbow trout *Oncorhynchus mykiss* during fast-starts and sprinting. *J. Exp. Biol.* **204**, 2239-2250.

Fernandez, D. A., Calvo, J., Wakeling, J. M., Vanella, F. A. and Johnston, I. A. (2002). Escape performance in the sub-Antarctic notothenioid fish *Eleginops maclovinus*. *Polar Biol.* **25**, 914-920.

Foreman, M. B. and Eaton, J. K. (1993). The direction change concept for reticulospinal control of goldfish escape. *J. Neurosci.* **13**, 4101-4113.

Frith, H. R. and Blake, R. W. (1991). Mechanics of the startle response in the northern pike, *Esox lucius*. *Can. J. Zool.* **69**, 2831-2839.

Gemballa, S. and Vogel, F. (2002). Spatial arrangement of white muscle fibers and myospetal tendons in fishes. *Comp. Biochem. Physiol. A.* **133**, 1013-1037.

Hale, M. E., Long, J. H., McHenry, M. J. and Westneat, M. W. (2002). Evolution of behavior and neural control of the fast-start escape response. *Evolution*. **56**, 993-1007.

James, R. S., Cole, N. J., Davies, M. L. F. and Johnston, I. A. (1998). Scaling of intrinsic contractile properties and myofibrillar protein composition of fast muscle in the fish *Myoxocephalus scorpius* L. *J. Exp. Biol.* **201**, 901-912.

Jayne, B. C. and Lauder, G. V. (1993). Red and white muscle activity and kinematics of the escape response of the bluegill sunfish during swimming. *J. Comp. Physiol. A* **173**, 495-508.

Jayne, B. C. and Lauder, G. V. (1995). Speed effects on midline kinematics during steady undulatory swimming of largemouth bass, *Micropterus salmoides. J. Exp. Biol.* **198**, 585-602.

Johnston, I. A., Franklin, C. E. and Johnson, T. P. (1993). Recruitment patterns and contractile properties of fast muscle fibers isolated from rostral and caudal myotomes of the short-horned sculpin. *J. Exp. Biol.* **185**, 251-265.

Johnston, I. A., van Leeuwen, J. L., Davies, M. L. F. and Beddow, T. (1995). How fish power predation fast-starts. *J. Exp. Biol.* **198**, 1851-1861.

Kasapi, M. A., Domenici, P., Blake, R. W. and Harper, D. G. (1993). The kinematics and performance of the escape response in the knifefish *Xenomystus nigri*. *Can. J. Zool.* **71**, 189-195.

Katz, S. L. and Shadwick, R. E. (1998). Curvature of swimming fish midlines as an index of muscle strain suggests swimming muscle produces net positive work. *J. Theor. Biol.* **193**, 243-256.

Katz, S. L., Shadwick, R. E. and Rappoport, H. S. (1999). Muscle strain histories in swimming milkfish in steady and sprinting gaits. *J. Exp. Biol.* **202**, 529-541.

Katz, S. L., Shadwick, R. E. and Syme, D. (2001). Enhanced power in yellowfin tuna. *Nature* **410**, 770-771.

Long, J. H., Jr, Adcock, B. and Root, R. G. (2002). Force transmission via axial tendons in undulating fish: a dynamic analysis. *Comp. Biochem. Physiol. A.* **133**, 911-929.

Rome, L. C., Funke, R. P., Alexander, R. M., Lutz, G., Aldridge, H., Scott, F. and Freadman, M. (1988). Why animals have different muscle fiber types. *Nature*. **355**, 824-827.

Shadwick, R. E., Steffensen, J. F., Katz, S. L. and Knower, T. (1998). Muscle dynamics in fish during steady swimming. *Am. Zool.* **38**, 755-770.

Shadwick, R. E., Katz, S. L., Korsmeyer, K. E., Knower, T. and Covell, J. W. (1999). Muscle dynamics in skipjack tuna: timing of red muscle shortening in relation to activation and body curvature during steady swimming. *J. Exp. Biol.* **202**, 2139-2150.

Stevens, K. K. (1987). *Statics and Strength of Materials* 2nd edn. New Jersey, USA: Prentice-Hall.

Tytell, E. D. and Lauder, G. V. (2002). The C-start escape response of *Polypterus senegalus*: bilateral muscle activity and variation during stage 1 and 2. *J. Exp. Biol.* **205**, 2591-2603.

Van Leeuwen, J. L., Lankheet, M. J. M., Akster, H. A. and Osse, J. W. M. (1990). Function of red axial muscle of carp (Cyprinus carpio): recruitment and normalized power output during swimming in different modes. *J. Zool. Lond.* **220**, 123-145.

Vogel, S. (2003). *Comparative Biomechanics*. Princeton, NJ: Princeton University Press.

Wainright, S. A., Vosburgh, F. and Hebrank, J. H. (1978). Shark skin: function in locomotion. *Science* **202**, 747-749.

Wakeling, J. M., (2001). Biomechanics of fast-start swimming in fish. *Comp. Biochem. Physiol. A.* **131**, 31-40.

Wakeling, J. M. and Johnston, I. A. (1998). Muscle power output limits fast-start performance in fish. *J. Exp. Biol.* **201**, 1505-1526.

Wakeling, J. M. and Johnston, I. A. (1999a). White muscle strain in the common carp and red to white muscle gearing ratios in fish. *J. Exp. Biol.* **202**, 521-528.

Wakeling, J. M. and Johnston, I. A. (1999b). Body bending during fast-starts in fish can be explained in terms of muscle torque and hydrodynamic resistance. *J. Exp. Biol.* **202**, 675-682.

Walker, J. A. (1998). Estimating velocities and accelerations of animal locomotion: a simulation experiment comparing numerical differentiation algorithms. *J. Exp. Biol.* **201**, 981-995.

Wardle, C. S. (1985). Swimming activity in marine fish. In *Physiological Adaptations of Marine Animals* (ed. M. S. Laverack), pp 521-540. Cambridge, UK: Company of Biologists.

Wardle, C. S., Videler, J. J., Arimoto, T., Francos, J. M. and He, P. (1989). The muscle twitch and maximum swimming speed of giant bluefin tuna, *Thunnus Thynnus* L. *J. Fish Biol.* **35**, 129-137.

Westneat, M. W., Hale, M. E., McHenry, M. J. and Long, J. H., Jr (1998). Mechanics of the fast-start: muscle function and the role of intramuscular pressure in the escape behavior of *Amia calva* and *Polypterus palma*. *J. Exp. Biol.* **201**, 3041-3055.

Webb, P. W. (1976). The effect of size on the fast-start performance of rainbow trout *Salmo gairdneri* and a consideration of piscivorous predatory–prey interaction. *J. Exp. Biol.* **65**, 157-177.

Webb, P. W. (1977). Effects of median-fin amputation on fast-start performance of rainbow trout (*salmon gairdneri*). *J. Exp. Biol.* **68**, 123-135.

Weihs, D. (1973). The mechanism of rapid starting of a slender fish. *Biorheology*. **10**, 343-350.

Wolfgang, M. J., Anderson, J. M., Grosenbaugh, M. A., Yue, D. K. P. and Triantafyllou, M. S. (1999). Near-body flow dynamics in swimming fish. *J. Exp. Biol.* **202**, 2303-2327.